



AIAA 96-1803

**Review of Blunt Body Wake Flows at
Hypersonic Low Density Conditions**

J. N. Moss and J. M. Price
NASA Langley Research Center
Hampton, VA 23681-0001

31st AIAA Thermophysics Conference
June 17-20, 1996/New Orleans, LA

REVIEW OF BLUNT BODY WAKE FLOWS AT HYPERSONIC LOW DENSITY CONDITIONS

James N. Moss* and Joseph M. Price**
Mail Stop 408A
NASA Langley Research Center
Hampton, VA 23681-0001

Abstract

Recent results of experimental and computational studies concerning hypersonic flows about blunted cones including their near wake are reviewed. Attention is focused on conditions where rarefaction effects are present, particularly in the wake. The experiments have been performed for a common model configuration (70° spherically-blunted cone) in five hypersonic facilities that encompass a significant range of rarefaction and nonequilibrium effects. Computational studies using direct simulation Monte Carlo (DSMC) and Navier-Stokes solvers have been applied to selected experiments performed in each of the facilities. In addition, computations have been made for typical flight conditions in both Earth and Mars atmospheres, hence more energetic flows than produced in the ground-based tests. Also, comparisons of DSMC calculations and forebody measurements made for the Japanese Orbital Reentry Experiment (OREX) vehicle (a 50° spherically-blunted cone) are presented to bridge the spectrum of ground to flight conditions.

Nomenclature

A base area of cone, $A = \pi d^2/4$
C_D drag coefficient, $C_D = 2D/\rho_\infty A$
C_H heat transfer coefficient, $C_H = 2q/\rho_\infty V_\infty^3$

$\overline{C_H}$ overall heat transfers coefficient,
 $\overline{C_H} = 2Q/\rho_\infty V_\infty^3 A$
C_p modified pressure coefficient,
 $C_p = 2p_w/\rho_\infty$
d_b base diameter
D drag
Kn Knudsen number, $Kn = \lambda/d$
M Mach number
n number density
p pressure
q heat transfer rate
Q overall (integrated) heat transfer
R_b cone base radius
R_c corner radius
R_n nose radius
Re_∞ Reynolds number, $Re_\infty = \rho_\infty V_\infty d/\mu_\infty$
s distance along the body surface
measured from the stagnation point
T_w surface temperature
u axial velocity
V freestream velocity
x axial distance from stagnation point
measured along symmetry axis
y radial distance from symmetry axis
λ mean free path
μ viscosity
ρ density

Subscripts

w surface values
∞ freestream values

Introduction

Since December 1991, the AGARD Fluid Dynamics Panel (FDP) has promoted¹ the activities of Working Group 18 (WG 18) to focus on a wide range of problems associated with hypersonic flows. One of the problems selected for investigation was the effect of rarefaction and real gas on blunt body wake flows. Interest in this particular problem arises from the complex flow features that evolve as the compressed forebody flow expands into the near wake. Flow features of importance for flight application include high-temperature effects (thermochemical nonequilibrium), rarefaction, separation, free shear layers, flow

* Research Engineer, Gas Dynamics Division, Fellow AIAA.

** Research Engineer, Gas Dynamics Division.

Copyright, 1996 by the American Institute of Aeronautics and Astronautics, Inc. No copyright is asserted in the United States under Title 17, U.S. Code. The U.S. Government has a royalty-free license to exercise all rights under the copyright claimed herein for Governmental purposes. All other rights are reserved by the copyright owner.

reattachment, and transition and turbulence at high Reynolds number conditions. Also, of issue are the conditions under which the near wake flow can become unsteady. Not only are these processes of fundamental importance, but also of practical importance for the design of planetary probes and aerobrake vehicles.

An objective of the WG 18 activity was to promote both experimental and computational studies such that the synergy would produce an enhanced understanding of the physical phenomena and a test of the computational capability to predict/model such phenomena. The blunt body wake problem was organized (see Ref. 1) as two subproblems: (1) high Reynolds number flows where the major emphasis would be on test conditions conducted in moderate to high enthalpy impulse facilities complemented with perfect gas wind tunnel data, and (2) low Reynolds number test conditions conducted in low-density wind tunnels, free jets, and high enthalpy impulse facilities by testing at either low pressure conditions or by using small models. The latter subproblem is the focus of the present review complemented with high altitude generic flight conditions for making code-to-code comparisons.

The forebody configuration for all experimental and flight conditions was a spherically blunted 70° half angle cone with an outer corner radius as shown in Fig. 1. The forebody configuration is the same as that for the Mars Pathfinder Probe scheduled for launch in December 1996 onboard a Delta II rocket; Mars arrival is planned for July 1997. The test models were supported with either an afterbody sting or small wires. Figure 2 displays the test conditions in terms of rarefaction as indicated by lines of constant $M_\infty/\sqrt{Re_\infty}$ where the characteristic dimension is the base diameter. The larger this parameter, the more rarefied the flow. As indicated, experiments have been performed in five different hypersonic facilities: (1) SR3 is a low density wind tunnel of the CNRS, Meudon, (2) V2G is a low density wind tunnel of the DLR, Göttingen, (3) V3G is a free jet facility at the DLR, Göttingen, (4) HEG is the world's largest free piston shock tunnel located at the DLR, Göttingen, and (5) LENS is the Large Energy National Shock tunnel located at Calspan, Buffalo. Results obtained with these five test facilities for the common model

(70° blunted cone) configuration are given in Refs. 2 through 11.

An extensive number of calculations have been performed for the experimental test conditions using direct simulation Monte Carlo (DSMC) and Navier Stokes (NS) solvers (Refs. 12-23). In addition, calculations have been reported for generic flight conditions for both Earth (Refs. 24-26) and Mars (Ref. 27) entry environments for the same forebody configuration with a base diameter of 2 meters.

The purpose of this review is to identify and summarize the extent of the experimental and computational data base currently available, identify significant findings, and identify gaps or possible deficiencies in the current data.

The final item discussed concerns comparisons between aerothermodynamic data extracted from the Japanese Reentry Experiment (OREX)^{28, 29} and computational findings²⁹⁻³³ under rarefied conditions. The DSMC comparisons with both the WG 18 test cases and the OREX data provide a broad spectrum of flow conditions for establishing a level of credibility for both the computational and experimental results.

Blunt Body/Wake Closure Experiments and Computations

A number of fundamental issues exist concerning such flows: how does the wake structure change as a function of rarefaction; what role does thermochemical nonequilibrium play in the near wake structure; and to what limits are continuum models realistic as rarefaction in the wake is progressively increased. In an effort to address these issues, as part of the AGARD WG 18 activity, both experiments and computations have been performed for the same forebody configuration: a 70° blunted cone with a nose radius equal to one-half the base radius and the corner or shoulder radius equal to 5 percent of the base radius (Fig. 1). Computations have been made for both wind tunnel and flight conditions for the same forebody configuration. Results of experiments performed in each of five hypersonic test facilities are briefly summarized along with some of the findings of the computational studies that have been made for specific test conditions.

The nominal test conditions for the low density wind tunnels participating in the AGARD WG 18 investigation are listed in Table 1. Also included are the test conditions for two impulse facilities. One test was run in the Large Energy National Shock Tunnel (LENS) facility^{10, 11} at a low pressure condition to produce Mach 15.6 nitrogen flow. Also, tests⁷ were conducted in the world's largest free piston shock-tunnel called the HEG (High Enthalpy Göttingen) using small models ($d_b = 5$ mm) and two of the test conditions in air are included in Table 1.

These test conditions provide a range of flow environments that include both nonreacting and reacting flows. Also, thermal nonequilibrium issues exist for even the lowest enthalpy tests (translational-rotational) with more internal nodes participating for the higher enthalpy flows. Hence, the conditions include a variety of flow environments that serve as excellent test cases to measure the ability of numerical schemes to calculate such flows where compression, expansion, and separation are key features.

SR3 Results

Reference 2 provides the most recent summary of the experiments conducted by the CNRS at Meudon, France using the SR3 wind tunnel. Three test conditions (Table 1) were considered where the freestream was nitrogen at a nominal Mach number of 20 and Reynolds numbers, based on model based diameter, ranging from 1,420 to 36,265. Three sets of data were obtained: density flowfields, heating rate distributions, and aerodynamic forces. Density flowfield measurements were made with the electron beam fluorescence technique for the two more rarefied conditions and for two angles of incidence: 0° and 10° . Heating rate distributions along forebody, base, and sting as well as aerodynamic forces are presented for angle of incidence between 0° and 30° .

The test models utilized had the same external dimensions and were sting supported. The model base diameter was 5 cm while the sting had a diameter of 1.25 cm and extended 7.5 cm downstream of the base plane before the sting cross sectional area began to increase (see Ref. 1, Chapter 4, Fig. 9). Details concerning the models, instrumentation, test procedures,

and tabulated and graphical presentations of results are given in Ref. 2.

A unique aspect of the SR3 tests was the density measurements which included flowfield values both with and without the model. The use of the nonintrusive electron beam fluorescence technique to provide measurements of the near wake and forebody density field provided the first such data for a generic aeroassist orbital transfer vehicle (AOTV) configuration.

An extensive number of computations have been made for the SR3 test conditions since the test parameters were defined well in advance of the actual experiments. Test condition 2 (Table 1) was a test case of the 4th European High-Velocity Database Workshop, ESTEC, Noordwijk, The Netherlands, Nov. 1994. Eight DSMC solutions were presented at this workshop and a summary of those results are given in Ref. 22.

Calculations using both DSMC and Navier-Stokes solvers were made either prior to the experiments (Refs. 12, 13, and 21 through 23, for example) or prior to release of the experimental data at the ESTEC Workshop²². Reference 14 provides an extensive presentation of information concerning flowfield features and surface quantities (including tabulated surface results) resulting from DSMC calculations. Also reported in Ref. 14 are the results of parametric studies concerning numerics (cell size and time step) and physical modeling (rotational collision number and surface reflection model).

Examples of the calculated and measured results for the SR3 tests are shown in Figs. 3-5. Examples of the surface heating distributions at zero incidence are presented in Fig. 3 for each of the three test conditions. As evident by the comparisons, the DSMC solutions¹⁷ show a better agreement with the measured values than do the Navier-Stokes^{34, 35} solutions (with surface slip and temperature jump boundary conditions) along the base plane and sting, regions where rarefaction effects are most significant. The agreement is outstanding along the sting and base plane since the measured signal along the base for Cases 1 and 2 were so small that the heating magnitude could only be characterized as being less than 0.002 and 0.004 W/cm² for Cases 1 and 2, respectively (indicated by symbol with downward pointing arrows in Fig. 3).

Along the forebody the agreement between calculated and measured results are not as good as expected¹⁷. Along the blunted cone forebody, the quality of the agreement between calculation and measurement decreases with decreasing rarefaction. This is most evident for Case 3 where the experimental value at $s/R_n = 1.56$ is 55 percent of the DSMC value. When the DSMC results along the forebody are compared with the Navier-Stokes solutions¹⁷, the agreement is 10 percent or better. Currently, the discrepancy observed in measured and computed heat transfer distributions along the forebody remain unresolved. Further experiments should be conducted to resolve this issue.

Figure 4 presents the measured and calculated heat transfer distributions were the calculated values are the 3-D solutions of Pallegoix²³ for incident angles of 0°, 10°, and 20°. Heat transfer measurements were made only along the windward ray. The agreement achieved is very good.

A number of computational studies have presented graphical results of the forebody and wake flow features demonstrating the influence of rarefaction on the flow structure. The DSMC calculations of Refs. 12 and 14 yield a wake vortex for each of the three test conditions with the size of the vortex increasing with decreasing rarefaction. Also, the location of maximum heating along the sting is downstream of the location of the free shear layer reattachment as indicated by the sting shear stress distribution.

As mentioned earlier, non-intrusive electron beam fluorescence measurements of the flowfield density were made² and Fig. 5 presents as an example a comparison of a DSMC calculation¹⁷ with measured values. (See Ref. 20 for even better agreement of computed and calculated results and Ref. 23 for comparisons at 10° incidence.) The measured results are presented as the ratio of local density with model to freestream values without model since density gradients exist in the undisturbed flow. The calculated results are local values ratioed to the freestream value (Table 1). The overall quantitative features of the two data sets are similar with the exception of the expansion of the flow about the outer corner of the model and the sudden up-turn of the 0.5 density contour adjacent to the sting.

The calculated density contours in the near wake show a concentrated expansion from the rewarded facing portion of the outer corner. This behavior is consistent with other DSMC calculations that have been made for Case 2 as summarized in Ref. 22, both at 0° and 10° incidence. The measurements show a more diffuse expansion extending down the base of the model. Part of this discrepancy may be due in part to a measurement resolution issue, since the gradients in density are substantial near the surface and occur in a rather small volume. As suggested in Ref. 22, the up-turn of the measured density contours along the sting are most likely due to an increase in the cross sectional area of the sting starting 80.4 mm downstream of the forebody stagnation point of the model. The change in the sting configuration was not included in the numerical simulations; however, a numerical simulation accounting for the change in sting configuration, even if approximate, would be instructive.

The aerodynamic forces, moments, and center of pressure were also measured for each flow condition at six angles of incidence spanning 0° and 30°. Tabulated results of these measurements are presented in Ref. 2. As reported in Ref. 17, the maximum difference in the measured and DSMC calculated drag coefficients for zero incidence was 6 percent. Reference 23 presents DSMC results for axial, normal, pitching moment, and center of pressure results for Case 2 flow conditions at 0°, 10°, and 20° incidence. The discrepancies with measured values are 11 percent or less.

V3G Results

An experimental test program⁷ has also been conducted for the 70° blunted cone with the V3G free-jet facility of the DLR Göttingen. Drag, lift, global heat transfer, and recovery temperature were measured in a Mach 9 nitrogen free-jet flow. These measurements were made for various degrees of rarefaction by including most of the transitional regime ($0.03 < Kn_0 < 6$) for stagnation temperatures of 300 K and 500 K. The wall-to-stagnation temperature ratio was varied between 0.8 and 1.5. The copper model with a base diameter of 5 mm was suspended with a thermocouple at angles of attack of $\alpha = 0^\circ, 20^\circ, \text{ and } 40^\circ$. Details concerning the experiments, data reduction, data accuracy, and results are included in Ref. 3.

Results for $T_0 = 300$ K, $T_w/T_0 = 1.0$ and zero incidence are presented in Figs. 6(a) and 6(b) for the drag and overall heat transfer coefficient ($\overline{C_H} = 2Q/\rho_\infty V_\infty^3 A$), respectively. The overall accuracy of the experiments was estimated³ to be ± 8 percent for these conditions. The DSMC solutions of Refs. 18 and 19 are in very good agreement with the experimental results.

V2G Results

The vacuum wind tunnel V2G at DLR, Göttingen has been used extensively to support the blunt body/wake research. Both qualitative and quantitative data have been reported in Refs. 5 through 7 for models with and without sting. The experiments were conducted in rarefied nitrogen flow at a nominal Mach number of 16 (see Table 1). Calibration results for the 15° half angle conical nozzle used to produce the flow is reported in Ref. 4. Reference 6 details much of the qualitative results obtained for 50 and 25 mm base diameter models with and without (wire suspension) stings. The data includes high frequency glow discharge flow visualization showing the shock shape, oil flow pictures giving surface streamlines, liquid crystal surface temperature visualization providing lines of constant temperature (lines of constant heat transfer under certain restrictions), and pitot pressure measurements in the wake. Data obtained with 5 mm base diameter model is included in Ref. 7.

Reference 6 and 8 describe the experiments conducted in V2G utilizing the Patterson probe to extract molecular flux information within the wake as a function of location and view direction. The 5 cm base diameter models suspended at zero incidence by three tungsten wires of 0.1 mm diameter were used in this study. The measurements show that a vortex is established for the most rarefied case (Case 1) and increases in length with decreasing Knudsen number. This is consistent with the DSMC calculated vortices included in Appendix A of Ref. 5. Figure 7 presents calculated and measured results for test Case 2 ($P_0 = 5$ bars) indicating good agreement for the wake centerline number flux, nu , ratioed to the freestream flux, $(nV)_\infty$. The agreement is good in terms of both the extent of separation and the magnitude of the molecular fluxes. A more

extensive presentation of the features of the wake flow including the non-Maxwellian behavior of the distribution function for these test conditions are given in Ref. 8 where DSMC calculations are compared with the measurements.

HEG Results

A series of experiments has been conducted at the DLR Göttingen with a 70° blunted cone having a base diameter of 15.24 cm. These tests have contributed to the high enthalpy, high Reynolds number portion of the WG 18 activity. Reference 7 describes several tests that have been conducted in air with enthalpies of 10 to 23 MJ/kg at freestream Mach numbers of approximately 10. For some of these tests, an array of four small models, 5 mm in diameter, were tested simultaneously with the larger model. The small models were located off centerline of the nozzle axis as was the large model. Objectives of the small model tests were to assess different heating rate measurement techniques as well as to obtain heating rate data along the forebody. Details concerning the experiments, models, and data reduction are given in Refs. 7 and 9. Reference 7 presents the freestream conditions including the freestream gas composition as calculated with a one-dimensional nonequilibrium nozzle code for nine tests conditions. Table 1 lists the freestream conditions for two of these tests [shots 132 (Case 1), and 131 (Case 2)] for which DSMC calculations have been made. The calculations were made using a 5-species reacting air gas model. For the lower enthalpy condition (Case 1), the maximum mole fraction of atomic nitrogen behind the bow shock was of the order of 0.01 while the value for Case 2 was of the order of 0.2. The calculated heating rate distributions for both cases are presented in Fig. 8 where the surface is assumed to be non-catalytic at a cold wall temperature of 300 K. Also shown are the measured results⁷ at the stagnation point and an s/R_N location of 0.6. Good agreement is obtained for both shots concerning the distributions and absolute values.

The estimated⁷ error of the heat transfer measurements for the small cone tests is ± 25 percent. The scatter as shown in Ref. 7 is within ± 20 percent.

LENS Results

As with the HEG experiments, several series of experiments have been conducted at Calspan with the large ($d_b = 15.24$ cm) blunted cone models. Tests have been made with the LENS facility using both nitrogen and air as test gases. Tests at both 5 and 10 MJ/kg conditions have been completed. Measurements consist of surface pressure and heating rates along the forebody, base, and sting. The focus of these tests are at continuum conditions; however, one test has been made at low pressure conditions where rarefaction effects should be evident in the wake. The specifics of this test condition are listed in Table 1. Results of the experimental measurements for the low pressure test were presented in Ref. 10 and DSMC results for this test condition have been reported in Refs. 10, 11, 15, and 17. Figures 9 and 10 present comparisons of calculated surface quantities for heating rate and pressure. The current DSMC results are compared with predictions obtained by Hash using an implicit, 3-temperature Navier-Stokes solver³⁶⁻³⁷. The slip boundary conditions used are those discussed in Ref. 38. The overall agreement is shown to be good, particularly along the sting. Largest differences occur along the base plane. The implication of the present comparison is that a Navier-Stokes solver can provide an adequate prediction of surface quantities for the current test problem.

Also shown in Figs. 9 and 10 are comparisons of measured and calculated values. As evident, there is good agreement between the calculations and experiments, both in the separated region and toward the end of the recompression process, indicating¹⁰ that the size of the base flow region is well predicted. The agreement between the experiment and calculations along the forebody are not as good. The experimental pressure values are anomalously high (yielding a stagnation pressure coefficient of $C_p = 3.0$), and should be disregarded³⁹ since the range of the pressure sensors were not appropriate along the forebody for this test. With only two heat transfer measurements along the forebody, it is not possible to establish the experimental trend for the heat transfer distribution.

Results for Generic Flight Conditions

The flight test cases consist of four individual cases to provide code-to-code comparisons for a 70° blunted cone with a 2 m base diameter. No experimental results are available for these test cases. The test cases are for both Earth and Mars entry using both reacting and nonreacting gas models. The freestream and surface boundary conditions are specified in Ref. 1 and listed in Table 2. These conditions correspond to altitudes of approximately 85 and 68 km in the Earth and Mars atmospheres, respectively. Only results for Earth entry conditions have been reported (Refs. 24-26); however, Ref. 27 has presented results for conditions similar to the Mars test case, the only difference being that the freestream number density is 0.727 percent of the test case value and the wake is not included. Findings from these computational studies follow.

Reference 24 presented results for both the reacting and nonreacting air test cases calculated with the DSMC method and also reacting air solutions using an axisymmetric 3-temperature, 5-species implicit Navier Stokes solver³⁶. The DSMC and Navier-Stokes results (Ref. 24) were in close agreement for the wake flow field quantities. Also, the size of the vortex as measured from the base of the blunted cone to the wake stagnation point is identical for the two solutions (Ref. 24). However, there are some noticeable differences in the chemical composition within the wake. The most significant difference between the two solutions is in the surface heating calculations along the base plane (Fig. 11). The Navier-Stokes results are 25 to 200 percent greater than the DSMC results, while good agreement exists along the forebody. When the calculation is made for nonreacting air as was done in Ref. 24, the results compared with the reacting air solution shows: much higher surface heating rates, particularly along the base plane (240 percent higher); a smaller vortex; similar values for the wake density contours and essentially the same value for drag.

DSMC solutions along the forebody are also included in Ref. 26 for this test case, where a different chemical reaction model is used compared to that of Ref. 24. Reacting and nonreacting results are presented showing the effect of the chemistry on stagnation

temperature and density profiles, but not on heating rates. The reacting heating rate results are somewhat higher, particularly in the stagnation region, when compared to that of Ref. 24. Comparison of the nonreacting heating results for these two different solutions would be useful.

For Mars entry conditions, Ref. 27 presents forebody solutions with and without chemical reactions for the CO₂ and N₂ freestream gas mixture (Table 2). Comparison between the two cases provide an indication of the effect of non-equilibrium chemical reaction on flowfield quantities and surface heating. The calculated effect on surface heating is very significant as is shown in Fig. 12. The heating rates for the nonreacting gas are of the order of three to four times the reacting gas results, showing that the chemistry has a much larger impact on forebody heating than for the air test case.

Additional calculations are needed for the generic flight test cases, particularly the Mars test case, to assess the differences among solution methods as well as the modeling issues associated with nonequilibrium chemistry. Solutions with and without chemical reactions helps to isolate differences that might exist among solutions. A critical discriminator is the surface heating.

Comparison with Flight

A major benefit of combined experimental/computational studies is often the sanity check one provides the other. A goal of the computational effort is to demonstrate capability for various test cases to enhance the reliability of calculations for actual flight conditions. This section will comment on recent applications of one of the DSMC codes⁴⁰ that has been applied to several of the previously discussed test cases to a flight experiment. This was the Japanese Orbital Reentry Experiment (OREX) vehicle which was a 50° half angle, spherically blunted cone with a base diameter of 3.4 m, a nose radius of 1.35 m, and a shoulder corner radius of 0.1 m.

OREX was flown in February of 1994 and initial results from this experiment are discussed in Refs. 28 through 31. The authors are not aware of any base heating or wake flow measurements made for the OREX.

Results of DSMC calculations that span the transitional flow regime (200 to 80 km) are

presented in Refs. 32 and 33 where comparisons are made with flight inferred data and continuum calculations. Comparisons of DSMC results with OREX results were made for acceleration, surface pressure, and stagnation-point heating rates. In general, the comparisons show good agreement. For acceleration, the agreement is good (Fig. 13). The surface pressure data are in qualitative agreement (see Ref. 33). Calculated and measured surface pressure values are in good quantitative agreement for the lower altitudes but depart with increasing altitudes as they should due to the high degree of nonequilibrium that exists at and within the inlet system used for the "measured pressures". This is a situation where the inlet measured pressure can be substantially less than the surface pressure.

Agreement for calculated and measured stagnation-point heating rates is fair. Figure 14 presents the flight inferred stagnation-point heating rate results as a function of time from launch of OREX. Continuum results obtained with viscous shock layer (VSL)³⁹ and Navier-Stokes³¹ solutions are shown for altitudes of 105 km to 48.4 km. The VSL results were for a no-slip and a non-catalytic surface. The DSMC results shown for 105 to 79.9 km included the finite catalytic wall boundary conditions used in the VSL calculations; however, the finite catalytic and non-catalytic boundary conditions yield essentially the same results over this altitude range (see Ref. 32). Inclusion of slip boundary conditions at the higher altitudes yield substantially lower heating rates for a continuum solution as is discussed in Ref. 32. The heating rates are inferred from the temperature measurements made on the back surface of a carbon-carbon material. As additional data are reported, opportunities will exist for comparing calculated and measured results at various locations along the forebody. The overall good correspondence of flight and calculated results is encouraging.

Concluding Remarks

A review of recent experimental and computational studies focused on blunt body forebody and wake flows is presented where the emphasis is on rarefied flows. An objective of this AGARD Fluid Dynamics Working Group 18 problem was to determine how the near wake

structure is influenced by rarefaction and real gas effects. The approach to achieve this objective was to select a generic blunt body configuration (70° spherically blunted cone) and encourage experimental contributions from the AGARD community. Once the experimental conditions were defined or conducted, computational contributions were solicited for the various experiments along with two generic flight conditions for entry into the atmosphere of Earth and Mars.

A key aspect of the success of this activity has been the experimental contributions from five hypersonic facilities that have fostered a significant number of computational contributions. The synergy of the computational/experimental activities has produced a significant data base that can serve as a valuable aid for aerobraking mission designs. Some of the key contributions or findings of this activity are: (1) first experimental measurements of density field and number flux for a generic Aeroassist Space Transfer Vehicle configuration; (2) data base involving both quantitative and qualitative information that spans a wide range of conditions (nonreacting to reacting flows) in the transitional regime; (3) demonstrated capability of different DSMC codes to simulate selected test cases (SR3, Condition 2); (4) the experimental (V2G, Patterson probe) and computational findings which show that the size of the wake vortex increases with decreasing Knudsen number; (5) the maximum heating along a sting/afterbody for zero incidence was of the order of five percent of the forebody stagnation value; (6) the location of wake reattachment and maximum sting heating rate are not coincident, but the separation between the two locations decrease with decreasing rarefaction; (7) inclusion of slip boundary conditions in the Navier-Stokes solvers provided improved agreement with experimental and DSMC results; (8) results from the Navier-Stokes solutions suggest that the overall Knudsen number should be less than about 0.001 before good agreement is achieved between experiment or DSMC for the near wake surface and flow features, and that the Navier-Stokes solutions agree with the DSMC results for quite large overall Knudsen numbers along the forebody; and (9) for the generic flight test cases which involve substantial dissociation, the calculated forebody and afterbody heating for

the reacting solutions are substantially less than for the corresponding nonreacting cases.

Readily evident from the above findings and the comparisons with the OREX flight measurements is a demonstrated capability of the DSMC method to calculate complex flow features including surface heating to good accuracy when compared to experimental measurements, both ground based and flight.

References

- ¹Anon., "Hypersonic Experimental and Computational Capabilities: Improvement and Validation," AGARD AR-319, vol. 1, May 1996.
- ²Allegre, Jean and Bisch, Daniele, "Blunted Cone at Rarefied Hypersonic Conditions - Experimental Density Flowfields, Heating Rates, and Aerodynamic Forces," CNRS Report RC 95-2, September 1995.
- ³Legge, Hubert, "Heat Transfer and Forces on a Blunted 70 Deg. Half Angle Cone Measured in Hypersonic Free Jet Flow," DLR Report IB 222-93 A 33, November 1993.
- ⁴Legge, H.; von Roden, G.; Klotzbach, A.; and Rammenzweig, D., "Calibration Data of V2G with a Conical Ma = 15 Nozzle," DLR IB 223-94A 11, 1994.
- ⁵Legge, Hubert, "Patterson Probe Measurements in the Wake of a 70 Deg. Half Angle Cone in Hypersonic Rarefied Flow," DLR Report-IB 223-94 A 15, December 1994.
- ⁶Legge, Hubert, "Flow Visualization and Pitot Probe Measurements in Hypersonic Rarefied Flow Around a 70 Deg. Half Angle Cone," DLR Report IB 223-95 A 01, February 1995.
- ⁷Legge, H., "Experiments on a 70 Degree Blunted Cone in Rarefied Hypersonic Wind Tunnel Flow," AIAA Paper 95-2140, June 1995.
- ⁸Danckert, A. and Legge, H., "Wake Structure of a 70 Degree Blunted Cone, DSMC Results, and Patterson Probe Measurements," AIAA Paper 95-2141, June 1995.

⁹Legge, H.; Rammenzweig, D.; and Klotzbach, A., "Heat Transfer Measurements on a Blunted 70 Deg Half Angle Cone in High Enthalpy Small Reynolds Number Flow," DLR Report IB 223-95 A 22, March 1996.

¹⁰Holden, M.; Kolly, J.; and Chadwick, K., "Calibration, Validation, and Evaluation Studies in the LENS Facility," AIAA Paper 95-0291, 1995.

¹¹Holden, M. S.; Chadwick, K. M.; Gallis, M. A.; and Harvey, J. K., "Comparison Between Shock Tunnel Measurements on a Planetary Probe Configuration and DSMC Predictions," 20th ISSW, Cal Tech, July 1995.

¹²Moss, J. N.; Mitcheltree, R. A.; Dogra, V. K.; and Wilmoth, R. G., "Direct Simulation Monte Carlo and Navier-Stokes Simulations of Blunt Body Wake Flows," AIAA Journal, vol. 32, no. 7, 1994, pp. 1399-1406.

¹³Wilmoth, R. G.; Mitcheltree, R. A.; Moss, J. N.; and Dogra, V. K., "Zonally Decoupled Direct Simulation Monte Carlo Solutions of Hypersonic Blunt-Body Wake Flows," Journal of Spacecraft and Rockets, vol. 31, no. 6, Nov. - Dec. 1994, pp. 971-979.

¹⁴Moss, J. N.; Dogra, V. K.; and Wilmoth, R. G., "DSMC Simulations of Mach 20 Nitrogen Flows about a 70° Blunted Cone and its Wake," NASA TM-107762, August 1993.

¹⁵Moss, J. N.; Price, J. M.; and Dogra, V. K., "DSMC Calculations for a 70° Blunted Cone at 3.2 km/s in Nitrogen," NASA TM-109181, January 1995.

¹⁶Dogra, V. K.; Moss, J. N.; Taylor, J. C.; Hash, D. B.; and Hassan, H. A., "Rarefaction Effects on Blunt-Body Wake Structure," Rarefied Gas Dynamics 19, edited by J. Harvey and G. Lord, Oxford University Press, 1995, pp. 1154-1160.

¹⁷Moss, J. N.; Dogra, V. K.; Price, J. M.; and Hash, D. B., "Comparison of DSMC and Experimental Results for Hypersonic External Flows," AIAA Paper 95-2028.

¹⁸Gallis, M. A. and Harvey, J. K., "Comparison of the Maximum Entropy DSMC Code with Flowfield Measurements," AIAA Paper 95-0413, 1995.

¹⁹Gallis, M. A. and Harvey, J. K., "Validation of DSMC Computations for the Flowfield Around a 70° Blunted Cone," Rarefied Gas Dynamics 19, edited by J. Harvey and G. Lord, Oxford University Press, 1995, pp. 1284-1290.

²⁰Marriott, R. M. and Bartel, T. J., "Comparison of DSMC Flow Field Predictions using Different Models for Energy Exchange and Chemical Reaction Probability," Rarefied Gas Dynamics 19, edited by J. Harvey and G. Lord, Oxford University Press, 1995, pp. 413-419.

²¹Gilmore, Martin R., "Rarefied Flow Over a Blunt Body," DRA/DWS/WX7/TR 95 189, February 1995.

²²Coron, F. and Harvey, J. K., "Synopsis for Test Case 6 - Rarefied 70° Spherically Blunted Cone," 4th European High-Velocity Database Workshop, ESTEC, Noordwijk, The Netherlands, Nov. 1994.

²³Pallegoix, J. F., "Workshop ESTEC--Test Case No. 6--Rarefied Spherically Blunted Cone," Paper presented at 4th European High-Velocity Database Workshop, ESTEC, Noordwijk, The Netherlands, November 1994.

²⁴Dogra, V. K.; Moss, J. N.; Wilmoth, R. G.; Taylor, J. C.; and Hassan, H. A., "Effects of Chemistry on Blunt-Body Wake Structure," AIAA Journal, vol. 33, no. 3, 1995, pp. 463-469.

²⁵Dogra, V. K.; Moss, J. N.; Wilmoth, R. G.; Taylor, J. C.; and Hassan, H. A., "Blunt Body Rarefied Wakes for Earth Entry," Journal of Thermophysics and Heat Transfer, vol. 9, no. 3, July - Sept., 1995, pp. 464-470.

²⁶Gallis, M. A. and Harvey, J. K., "Implementation of a Maximum Entropy Method in Monte Carlo Direct Simulations," AIAA Paper 95-2094.

²⁷Gallis, M. A. and Harvey, J. K., "Analysis of Non-Equilibrium in Mars Atmosphere Entry Flows," AIAA Paper 95-2095.

²⁸NAL/NASDA Joint Research Report. OREX, March 1995 (in Japanese).

²⁹Inouye, Y., "OREX Flight- Quick Report and Lessons Learned," Invited paper 4, 2nd European Symposium on Aerothermodynamics of Space Vehicles, ESTEC, Nov. 1994.

³⁰Yamamoto, Y. and Yoshioka, M., "CFD and FEM Coupling Analysis of OREX Aerothermodynamic Flight Data," AIAA Paper 95-2087, June 1995.

³¹Yamamoto, Y., Private Communication, Aerodynamics Division, National Aerospace Lab., Tokyo-182, Japan, Dec. 1995.

³²Gupta, R. N., Moss, J. N., and Price, J. M., "Assessment of Thermochemical Nonequilibrium and Slip Effects for Orbital Reentry Experiment (OREX)," AIAA Paper 96-1859, June 1996.

³³Moss, J. N. and Price, J. M., "DSMC Calculations of OREX Entry," 20th International Symposium on Rarefied Gas Dynamics, Beijing, China, August 1996.

³⁴Gnoffo, P. A., "An Upwind-Biased, Point-Implicit Relaxation Algorithm for Viscous Compressible Perfect-Gas Flows," NASA TP-2953, February 1990.

³⁵Gnoffo, P. A.; Gupta, R. N.; and Shinn, J. L., "Conservation Equations and Physical Models for Hypersonic Air Flows in Thermal and Chemical Nonequilibrium," NASA TP-2867, Feb. 1989.

³⁶Olynick, D. R. and Hassan, H. A., "New Two-Temperature Dissociation Model for Reacting Flows," Journal of Thermophysics and Heat Transfer, vol. 7, no. 4, Oct. - Dec. 1993, pp. 687-696.

³⁷Olynick, D. R.; Taylor, J. C.; and Hassan, H. A., "Comparisons Between DSMC and the Navier-Stokes Equations for Reentry Flows," AIAA Paper 93-2810, July 1993.

³⁸Gupta, R. N.; Scott, C. D.; and Moss, J. N., "Slip-Boundary Equations for Multicomponent Nonequilibrium Airflow," NASA TP-2452, Nov. 1985.

³⁹Holden, M. S., Personal Communication, May 1995, Calspan Corporation, Buffalo, New York.

⁴⁰Bird, G. A., Molecular Gas Dynamics and the Direct Simulation of Gas Flows, Clarendon Press, Oxford, 1994.

⁴¹Gupta, R. N., "Viscous Shock-Layer Study of Thermochemical Nonequilibrium," Journal of Thermophysics and Heat Transfer, vol. 10, no. 2, 1996, pp. 257-266.

Table 1. Experimental Test Conditions

Test Case	T_0 (K)	P_0 (bars)	M_∞	Re_∞/cm	$\rho_\infty \times 10^5$ (kg/m ³)	V_∞ (m/s)	T_∞ (K)	λ_∞ (mm)	T_w (K)	Gas
(a) SR3 Wind Tunnel, CNRS Meudon; $d_b = 5$ cm										
1	1100	3.5	20.2	285	1.73	1502	13.3	1.59	300	N2
2	1100	10.0	20.0	838	5.19	1502	13.6	0.54	300	N2
3	1300	120.0	20.5	7277	46.65	1633	15.3	0.06	300	N2
(b) V2G Wind Tunnel, DLR Göttingen; $d_b = 5, 2.5, \text{ and } 0.5$ cm										
1	575	2	15.6	719	6.70	1082	11.6	0.39	490	N2
2	675	5	16.5	1233	11.02	1173	12.2	0.25	565	N2
3	775	10	16.8	1935	17.25	1257	13.4	0.16	635	N2
(c) V3G Wind Tunnel, DLR Göttingen, $d_b = 0.5$ cm										
1	295	0.163	9.0	859	14.22	759	17.2	0.16	variable	N2
2	295	0.0549	9.0	286	4.74	759	17.2	0.48	variable	N2
3	295	0.0163	9.0	86	1.42	759	17.2	1.60	variable	N2
4	295	0.0054	9.0	29	0.47	759	17.2	4.80	variable	N2
(d) HEG, DLR Göttingen; $d_b = 0.5$ cm										
1	6713	576.0	10.1	7043	408.5	4539	489.9	0.017	300	Air
2	9244	385.0	9.5	2498	156.4	6075	856.4	0.044	300	Air
(e) LENS, Calspan Buffalo; $d_b = 15.24$ cm										
1	4351	74.1	15.6	578	13.06	3246	103.7	0.35	294	N2

Table 2. Flight Test Conditions *

Quantity	Earth Entry	Mars Entry
Number density, m ⁻³	1.654 x 10 ²⁰	1.654 x 10 ²⁰
Temperature, K	180.65	141
Velocity	7.0	7.0
Mole fraction N ₂	0.7628	0.05
Mole fraction O ₂	0.2372	-----
Mole fraction CO ₂	-----	0.95

*70° blunted cone with base diameter of 2 m and a noncatalytic surface with a wall temperature of 1000 K.

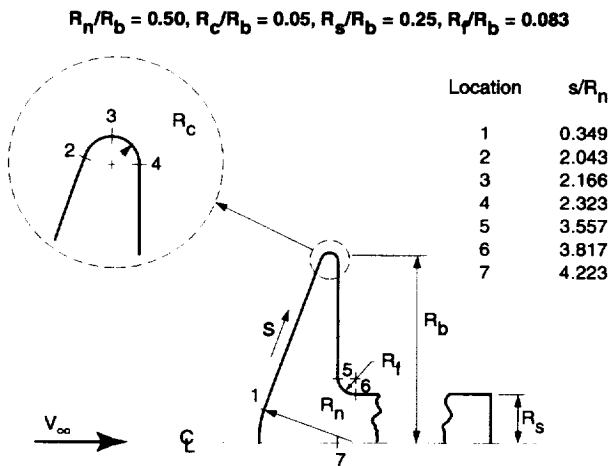
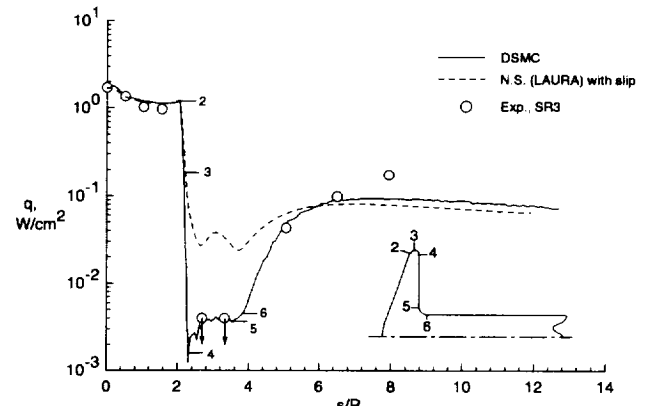


Fig. 1 70° spherically blunted cone configuration.



(b) Case 2.

Fig. 3 Continued.

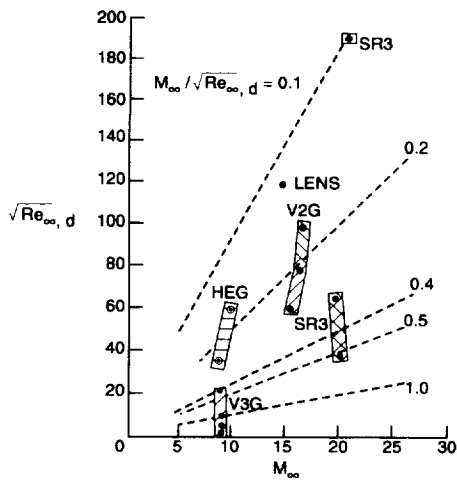
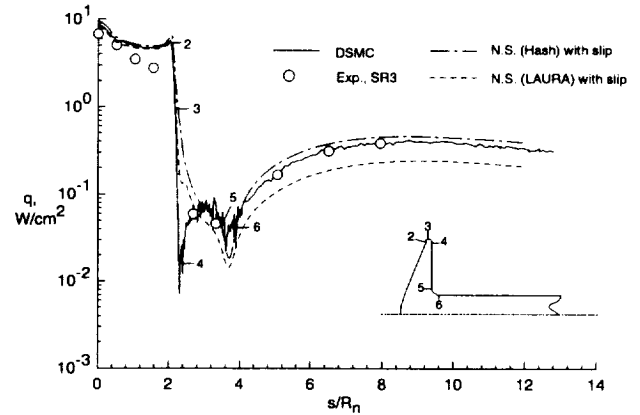
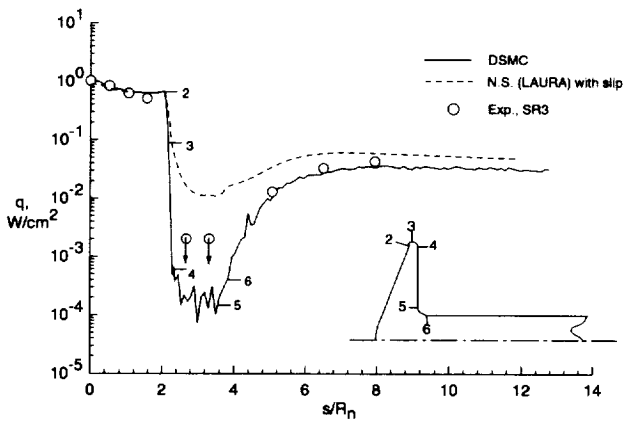


Fig. 2 Low-density test conditions in terms of the rarefaction parameter $M_\infty/\sqrt{Re_\infty, d}$.



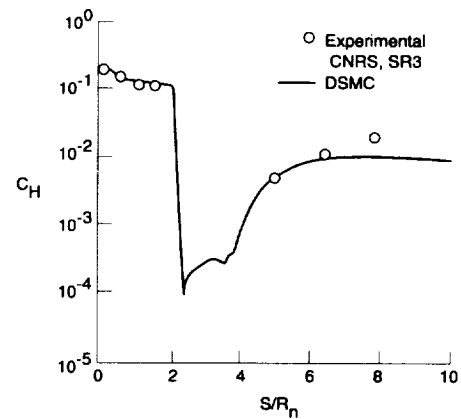
(c) Case 3.

Fig. 3 Concluded.



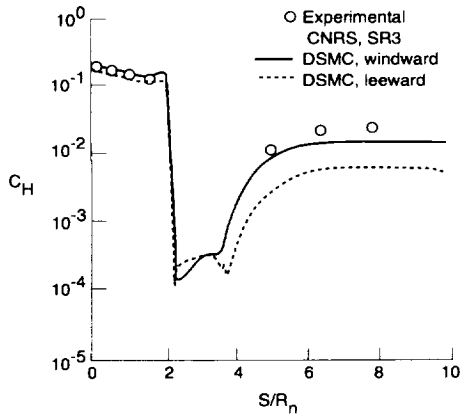
(a) Case 1.

Fig. 3 Comparison of SR3 experimental² and computed¹⁷ heating rate results ($d_b = 5.0$ cm).



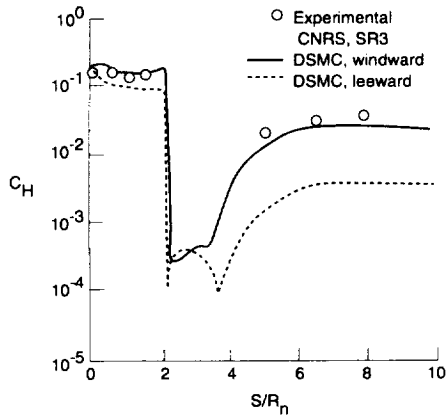
(a) Incidence = 0°.

Fig. 4 Comparison of SR3 experimental² and computed²³ heating rate distributions for Case 2



(b) Incidence = 10°.

Fig 4 Continued.



(c) Incidence = 20°.

Fig 4 Concluded.

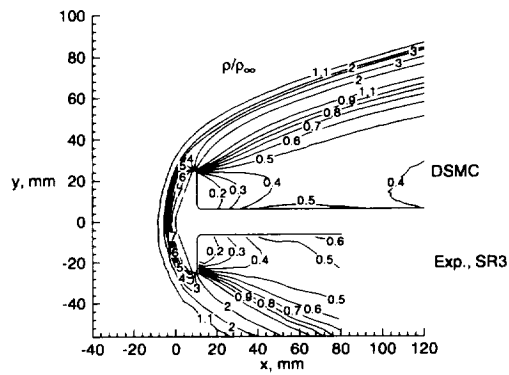
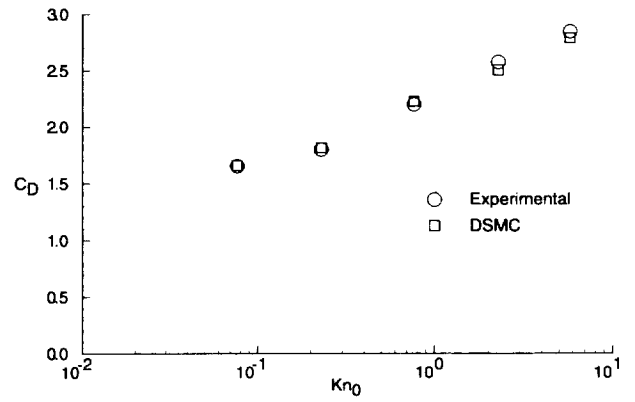
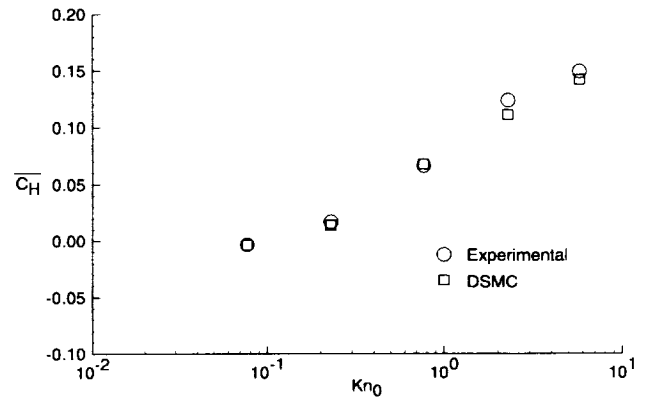


Fig. 5 Comparison of measured² and calculated¹⁷ density for SR3 test Case 2.



(a) Drag coefficient.

Fig. 6 Comparison of experimental³ and DSMC¹⁸⁻¹⁹ results for V3G tests with model at zero incidence.



(b) Overall heat transfer coefficient.

Fig. 6 Concluded.

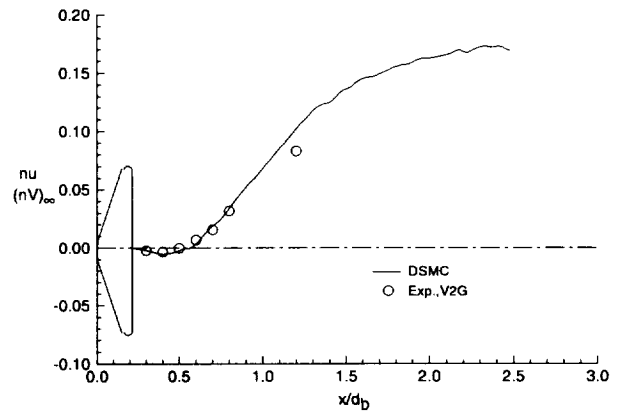


Fig. 7 Measured² and calculated¹⁷ number flux along centerline of near wake for V2G test Case 2.

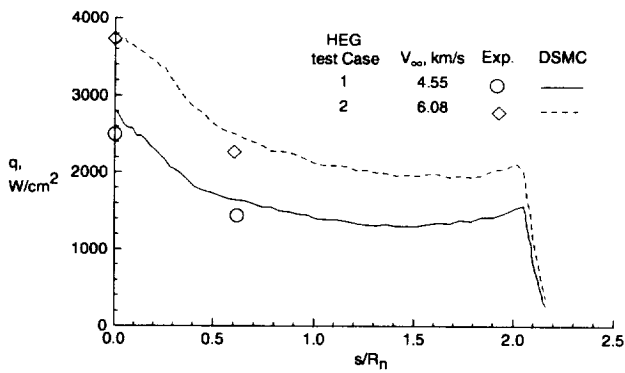


Fig. 8 Measured⁷⁻⁹ and calculated¹⁷ heating rates for two HEG tests using 5 mm base diameter models.

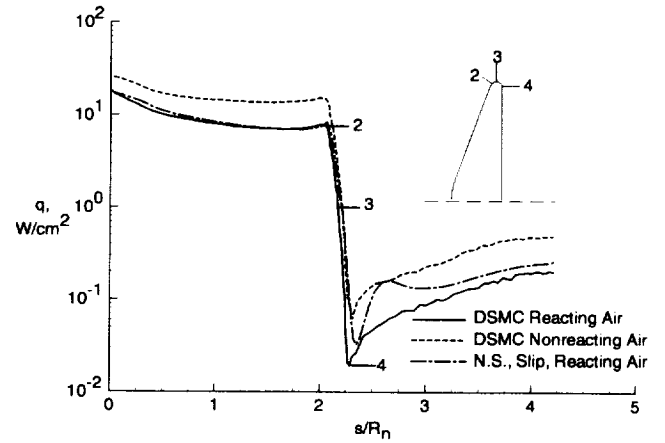


Fig. 11 Calculated²⁴ heating rate distributions for Earth entry (Alt = 85 km, $V_{\infty} = 7$ km/s, $d_b = 2.0$ m).

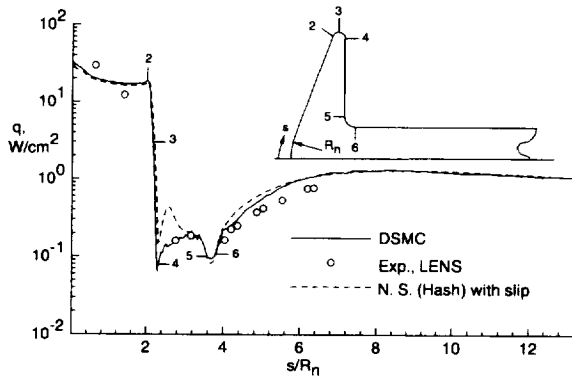


Fig. 9 Measured¹⁰ and calculated¹⁵ heating rate distributions for LENS test Case 1.

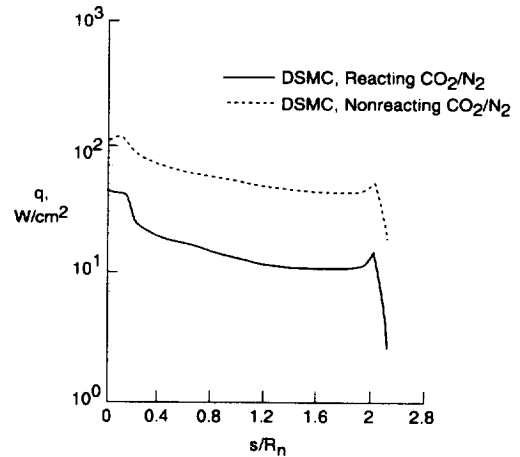


Fig. 12 Calculated²⁷ heating rate distributions for Mars entry (Alt = 68 km, $V_{\infty} = 7.0$ km/s, $d_b = 2.0$ m).

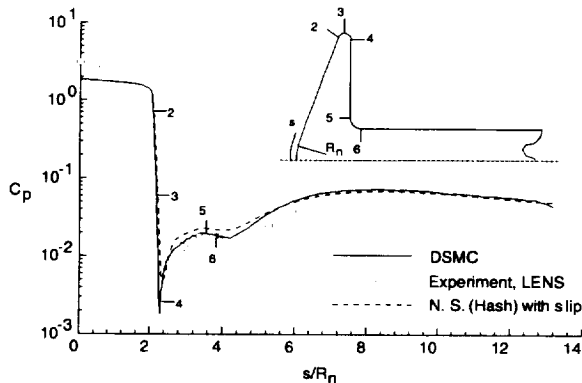


Fig. 10 Measured¹⁰ and calculated¹⁵ pressure distributions for LENS test Case 1.

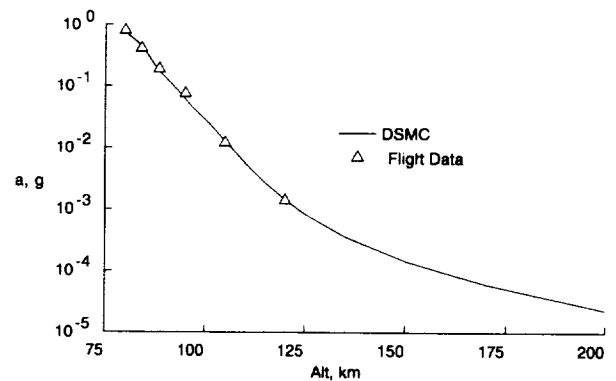


Fig. 13 Comparison of calculated³³ and measured²⁹ OREX axial acceleration.

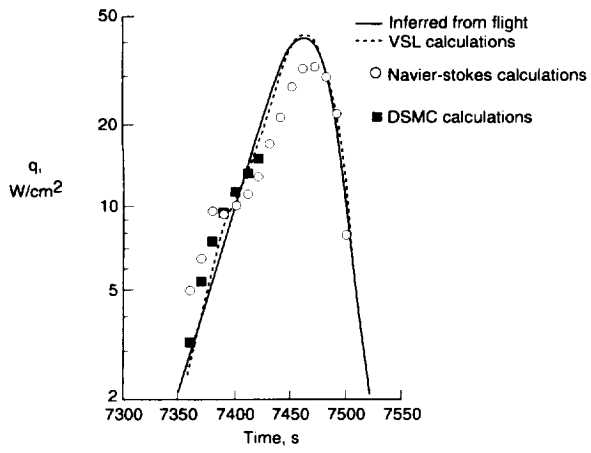


Fig 14. Comparison of flight inferred³⁰ stagnation-point heating rates with calculations using VSL³², NS³¹, and DSMC³²

